Materials Letters 234 (2019) 357–360

Contents lists available at ScienceDirect

Materials Letters

journal homepage: www.elsevier.com/locate/mlblue

Molecular dynamics simulation of double-layered graphene-carbon nanotube junctions for thermal rectification

Xueming Yang [a,*], Jiangxin Xu [a], Sihan Wu [a], Dapeng Yu [a], Bingyang Cao [b,*]

[a] Department of Power Engineering, North China Electric Power University, Baoding 071003, China
[b] Key Laboratory for Thermal Science and Power Engineering of Ministry of Education, Department of Engineering Mechanics, Tsinghua University, Beijing 100084, China

ARTICLE INFO

Article history:
Received 27 June 2018
Received in revised form 5 September 2018
Accepted 21 September 2018
Available online 22 September 2018

Keywords:
Carbon materials
Thermal rectification
Graphene-carbon nanotube junction
Local resonance
Molecular dynamics
Thermal properties

ABSTRACT

By using molecular dynamics simulations, we have studied the thermal rectification in double-layered Graphene-carbon nanotube (DGN-DWCNT) junctions. It is found that DGN-DWCNT junctions exhibit significant thermal rectification under both large and small thermal bias. Even under a small thermal bias $|\Delta| = 0.1$, a rectification ratio as high as 300.6% can be achieved. The influences of the geometric parameters on the thermal rectification of the DGN-DWCNT junctions are discussed, and the underlying mechanism of the significant thermal rectification is explored. These results open a door in the applicability of DGN-DWCNT junctions and their based pillared graphene system in nanoscale engineering of thermal transport devices.

© 2018 Elsevier B.V. All rights reserved.

1. Introduction

As a fundamental device for heat transport control and phononics, the thermal rectifier allows heat/phonon to flow preferentially in one direction. Thermal rectifiers have great potential in thermal management and phononics circuit applications [1,2]. To obtain a more efficient thermal rectifier, many studies have been conducted to explore new nanostructures with a TR effect and to study novel TR mechanisms [3–11]. Experimental study by Zhu et al. [12] demonstrated that the pillared graphene system (PGS) can be constructed by double-layered graphene connected with double-walled CNT (DGN-DWCNT). Although excellent rectification effect in some graded PGS and their building blocks have been reported [13,14], as a new PGS nanostructure, the thermal conduction of DGN-DWCNT junction has not been studied yet. In this letter, thermal rectification in DGN-DWCNT junctions is investigated by using classical non-equilibrium molecular dynamics (NEMD) simulations.

2. Simulations

The DGN-DWCNT junctions studied in this work are constructed with a GN-SWCNT(12,12) junction and a GN-SWCNT (6,6) junction; the atomic modeling and assembly process is depicted in Fig. 1a. The 3D view, aerial view, and front view of the structure diagram and atomic modeling of the DGN-DWCNT junction are respectively shown in Fig. 1b–d, where the red and green areas respectively denote the thermostated and fixed parts, and the left is the free parts. L_1 is the height from the top of the tube to the bottom of the square graphene nanosheet, and L_2 is the width of the square graphene nanosheet. The distance (δ_L) between the two layers of graphene nanosheet in the DGN-DWCNT junction is 3.4 Å. Along the tube's longitudinal direction, the side of the graphene nanosheets is hereafter referred to as the wide side, and the open end of the tube is referred to as the narrow side. All simulations in the present study are carried out by using the LAMMPS software package [15]. The optimized Tersoff potential [16] is adopted to model the sp^2 covalent bonding for graphene and CNT. The Lennard–Jones (LJ) potential is used to model the noncovalent vdW interaction between CNTs and graphene with the parameters of $\varepsilon = 0.004555$ ev and $\sigma = 3.851$ Å, taken from ref [17]. The cutoff distance for LJ potential is set at 2.5σ. The atoms in the fixed parts at both sides are fixed to obtain a suspended structure, and the free boundary condition is applied in all directions.

The system equilibrium is reached in the NVT ensemble at 300 K for 5×10^6 time steps with a Nosé-Hoover thermostat. Then, the system is switched to NVE ensemble, and classical NEMD is carried out for another 12×10^6 steps to establish a temperature

* Corresponding authors.
E-mail addresses: xuemingyang@ncepu.edu.cn (X. Yang), caoby@tsinghua.edu.cn (B. Cao).

https://doi.org/10.1016/j.matlet.2018.09.121
0167-577X/© 2018 Elsevier B.V. All rights reserved.

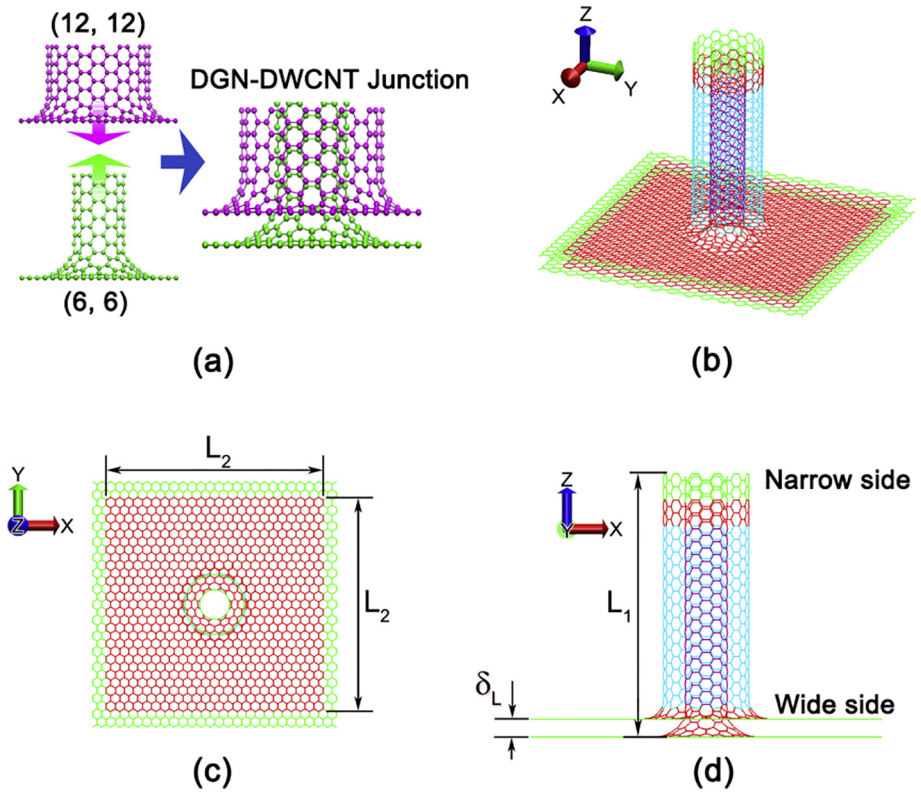

Fig. 1. The structure diagram of DGN-DWCNT junction. (a) Atomic modeling. (b), (c) and (d): 3D view, Aerial view and Front view, respectively.

gradient along the longitudinal direction of the tubes using a Berendsen thermostat [18]. Temperatures in the heat bath regions on the wide and narrow sides are respectively maintained at $T_0(1+\Delta)$ and $T_0(1-\Delta)$; T_0 is the average temperature, and Δ is the normalized temperature difference. The TR ratio can be computed as $\eta = \frac{(J_+ - J_-)}{J_-} \times 100\%$, where J_+ is the heat flux from the wide side to the narrow side when $\Delta > 0$, and J_- is the heat flux from the narrow side to the wide side when $\Delta < 0$.

The influence of L_1 and L_2 on the TR ratios of the DGN-DWCNT junctions is analyzed. MD simulations are carried out to obtain 2D gridded data of the TR ratio when L_1 varies from 3.69 to 9.84 nm (i.e., 15–40 unit cells) with a step of five unit cells, and L_2 varies from 6 to 18 nm with a step of 2 nm. In the simulations, T_0 is set at 300 K, and $|\Delta|$ is set at 0.5. Then, a smoother surface distribution of the TR ratio is obtained by cubic interpolation performed on the gridded simulation results. As can be seen from Fig. 2a and b, when L_1 = 6.1 nm and L_2 = 12 nm (geometry size sets A), the obtained maximum η of the DGN-DWCNT junctions reaches 737.6%. Here the maximum thermal rectification obtained is only for the limited geometry parameters size range. Moreover, it can be observed from the Fig. 2 that the variation of the TR ratio with the geometry parameters (L_1 and L_2) is fairly complicate, which is related with the temperature- dependent power spectrum and the nonlinear lattice dynamics.

Fig. 2(c) and (d) show respectively the TR ratio η and heat flux as a function of average temperature and $|\Delta|$ for DGN-DWCNT Junction with geometry size sets A. Although the TR ratio increases steadily with an increase of $|\Delta|$ in the range from 0.1 to 0.5, the increasing is not linear. Such a variation trend is different from those in GN-SWCNT(6, 6) junctions [14]. This difference may result from the coupling interaction by the inner GN-SWCNT(6,6) junction and the outer GN-SWCNT(12,12) junction in the DGN-DWCNT Junction. In fact, the variation trend of η with $|\Delta|$ is dependent on the structure of the system. Previous studies have presented different variation trend of η with $|\Delta|$ for different nanostructures, such as the linear increasing trend [4], the nonlinear increasing trend [5,6] and even decreasing trend [7]. DGN-DWCNT exhibit an advantage at a low$|\Delta|$, a rectification ratio as high as 300.6% is achieved even under a small thermal bias $|\Delta|$ = 0.1, which is much higher than the reported 188.6% of the GN-SWCNT(6,6) junctions[14].

To analyze the coupling effect in the DGN-DWCNT junction, the regional vibration density of states (vDOS) and the velocity autocorrelation function (VACF) for the wide and narrow sides are calculated for the entire DGN-DWCNT junction, the GN-SWCNT(12,12) junction part, and the GN-SWCNT(6,6) junction part, respectively, as shown in Fig. 3. For all these parts, it can be observed that the calculated regional vDOS of the wide and narrow sides of the system matches well under positive thermal bias, but mismatches obviously due to the significant peaks appeared at the narrow side under the negative thermal bias. The good match of the vDOS means the phonon can easily go through the system along the direction of temperature gradient and correspond to the larger heat flux; in contrast, when the power spectra of the different parts fail to sufficiently overlap, the phonon has difficulties to pass through the system, thus leading to suppressed heat transfer [19]. This match and mismatch of the spectra of lattice vibration can well explain the significant TR in the DGN-DWCNT junction.

For the entire DGN-DWCNT junction, significant sharp peaks at 14.3 THz and 28.6 THz appear under negative thermal bias in the vDOS at the narrow side (Fig. 3a). These sharp peaks are coincided with those in the vDOS for the GN-SWCNT(12,12) junction part (Fig. 3e). However, the frequencies of the peaks for the GN-SWCNT(6,6) junction part were 14.4 THz (Fig. 3i), slightly different from 14.5 THz previously reported for the single GN-SWCNT (6,6) junctions. This finding suggests that the GN-SWCNT(6,6) junction

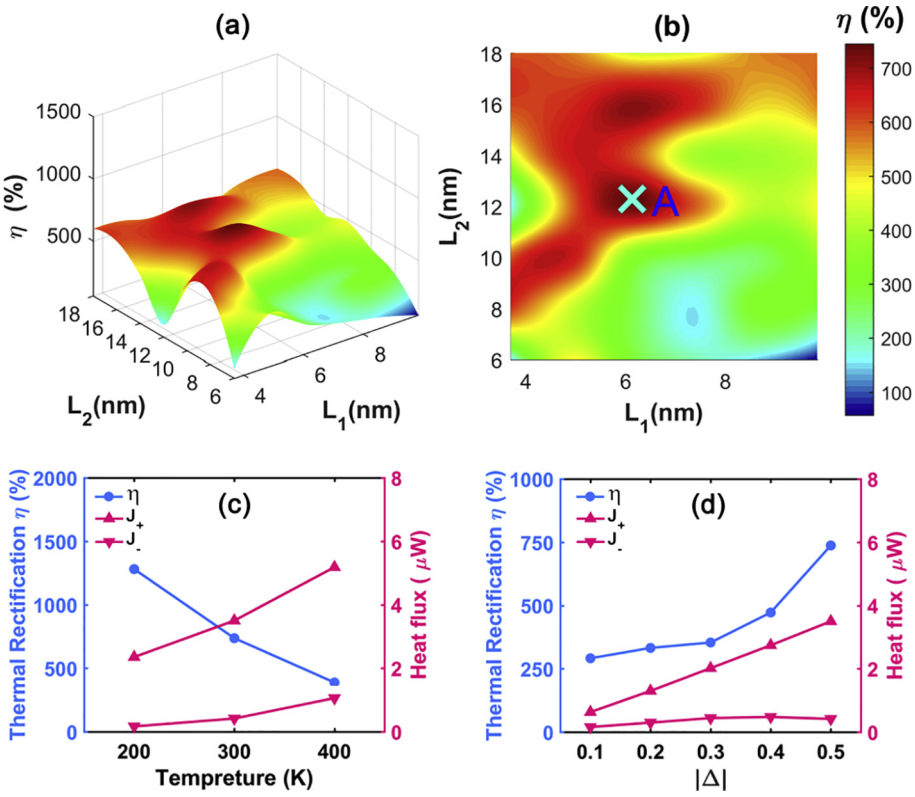

Fig. 2. (a) and (b) 3D and 2D view of the distribution of the TR ratio η with respect to a tube length L_1 and a side length of graphene nanosheet L_2 for DGN-DWCNT Jiunction; (c) TR ratio η and heat flux as a function of average temperature when $|\Delta| = 0.5$; (d) TR ratio η and heat flux as a function of $|\Delta|$ when the average temperature is 300 K.

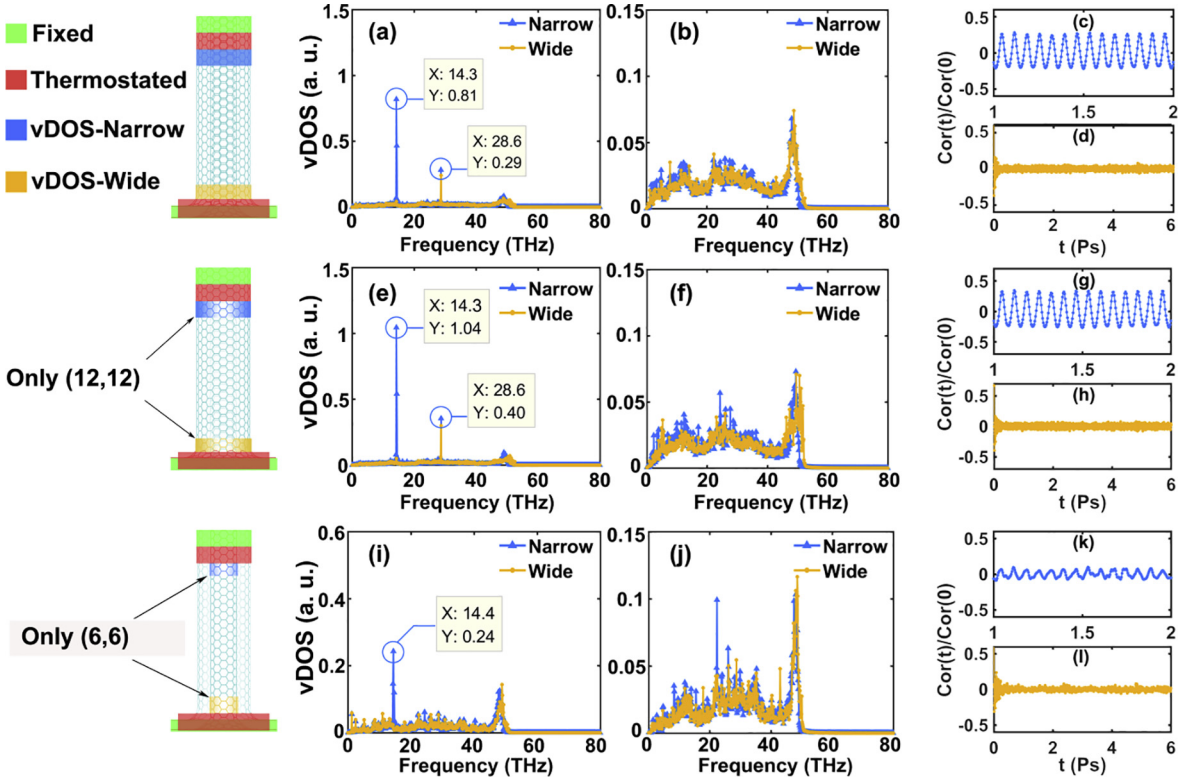

Fig. 3. vDOS per atom and VACF for the entire junction, the inner part and the outer part of the DGN-DWCNT Junction with L_1 = 6.1 nm and L_2 = 12 nm. (a), (e), and (i) vDOS when $\Delta = -0.5$; (b), (f), and (j) vDOS when $\Delta = 0.5$; (c), (g), and (k) VACF for narrow sides when $\Delta = -0.5$; (d), (h), and (l) VACF for wide sides when $\Delta = -0.5$.

part is restrained by the outer GN-SWCNT(12,12) junction, and its resonance is also depressed. The power spectra of the entire DGN-DWCNT junction is dominated by the outer (12, 12) junction, the peak of which exceeds that of the inner (6,6) junction.

Corresponding VACFs under $\Delta = -0.5$ are also calculated for the wide and narrow sides of the entire DGN-DWCNT junction, GN-SWCNT(12,12) junction part, and GN-SWCNT(6,6) junction part; refer to Fig. 3c, d, g, h, k and l, respectively. The periodicity of the VACF can be observed for all narrow sides, and the frequencies coincided with the sharp peaks in the corresponding VDOS, thus the significant peaks are demonstrated to be standing waves induced by local resonance. Such periodicity is not found for the wide sides. The waveform of VACF for the narrow side of the GN-SWCNT(6,6) junction part is less stable, and the amplitude is much smaller than that of the GN-SWCNT(12,12) junction part, indicating that the standing wave in GN-SWCNT(6,6) junction part is much weaker than that of the GN-SWCNT(12,12) junction part. The origin of standing wave is a resonance excited by the high temperature or the heat fluxes in the thermostated part [10,20], and the standing wave is essentially a kind of mechanical wave. In fact, studies [21–23] had shown that mechanical wave can be excited by the high heat flux. For the entire DGN-DWCNT junction, strong local standing wave appears near the tube ends and greatly hinders the propagation of phonon waves as well as the transfer of thermal energy under negative thermal bias.

3. Conclusions

In summary, thermal rectification in the DGN-DWCNT junctions is investigated via MD simulations. It is found that DGN-DWCNT junctions exhibit significant thermal rectification under both large and small thermal bias. Even under a small thermal bias $|\Delta| = 0.1$, a rectification ratio as high as 300.6% can be achieved. The influences of the geometric parameters on the thermal rectification are discussed, and the underlying mechanism of significant thermal rectification is explored. We find that the local standing waves in the junction under negative thermal bias should be responsible for the significant thermal rectification. In fact, due to the abundance of low-grade waste heat, high efficient thermal rectifier under small temperature differences should be more important than those under high temperature bias for real applications. Our results suggest that DGN-DWCNT junction is a promising candidate for future design of carbon-based thermal rectifier.

Acknowledgment

This research is supported by the National Natural Science Foundation of China (Grant No. 51576066).

References

[1] B. Li, L. Wang, G. Casati, Phys. Rev. Lett. 93 (2004) 184301.
[2] S. Hu, M. An, N. Yang, B. Li, Small 13 (2017).
[3] Y. Wang, A. Vallabhaneni, J. Hu, B. Qiu, Y.P. Chen, X. Ruan, Nano Lett. 14 (2014) 592–596.
[4] N. Yang, G. Zhang, B. Li, Appl. Phys. Lett. 95 (3) (2009) 033107.
[5] J.W. Jiang, J.S. Wang, B. Li, EPL: Europhys. Lett. 89 (4) (2010) 46005.
[6] X. Ni, G. Zhang, B. Li, J. Phys.: Condens. Mat. 23 (21) (2011) 215301.
[7] K. Gordiz, S.M. Vaez Allaei, F. Kowsary, Appl. Phys. Lett. 99 (25) (2011) 251901.
[8] T. Zhang, T. Luo, Small 11 (2015) 4657–4665.
[9] G. Lei, H. Cheng, H. Liu, W. Rao, Mater. Lett. 189 (2017) 101–103.
[10] Y.Y. Liu, W.X. Zhou, K.Q. Chen, Sci. Rep. 5 (2015) 17525.
[11] G. Zhang, H. Zhang, Nanoscale 3 (2011) 4604–4607.
[12] Y. Zhu, L. Li, C. Zhang, G. Casillas, Z. Sun, Z. Yan, R.H. Hauge, Nat. Commun. 3 (2012) 1225.
[13] X. Yang, D. Yu, B. Cao, A.C. To, ACS Appl. Mater. Inter. 9 (2017) 29–35.
[14] X. Yang, D. Yu, B. Cao, ACS Appl. Mater. Inter. 9 (2017) 24078–24084.
[15] S. Plimpton, J. Comput. Phys. 117 (1995) 1–19.
[16] L. Lindsay, D.A. Broido, Phys. Rev. B 81 (2010) 205441.
[17] A.K. Rappé, C.J. Casewit, K.S. Colwell, W.A. Goddard Iii, W.M. Skiff, J. Am. Chem. Soc. 114 (1992) 10024–10035.
[18] H.J. Berendsen, J.V. Postma, W.F. van Gunsteren, H.J. DiNola, J.R. Haak, J. Chem. Phys. 81 (1984) 3684–3690.
[19] N. Li, J. Ren, L. Wang, G. Zhang, P. Hänggi, B. Li, Rev. Mod. Phys. 84 (2012) 1045.
[20] X.K. Chen, Z.X. Xie, W.X. Zhou, L.M. Tang, K.Q. Chen, Carbon 100 (2016) 492–500.
[21] X. Zhang, M. Hu, D. Poulikakos, Nano Lett. 12 (7) (2012) 3410–3416.
[22] K. Zheng, L. Wang, S. Bai, J. Yu, Z. Tang, Z. Huang, Physica B 434 (2014) 64–68.
[23] B. Liu, J.A. Baimova, C.D. Reddy, S.V. Dmitriev, W.K. Law, X.Q. Feng, K. Zhou, Carbon 79 (2014) 236–244.